Dense magnetized plasma numerical simulations

2010 Plasma Sources Sci. Technol. 19 034024

(http://iopscience.iop.org/0963-0252/19/3/034024)

Plasma Sources Sci. Technol. **19** (2010) 034024 (6pp) doi:10.1088/0963-0252/19/3/034024

Dense magnetized plasma numerical simulations

L Bilbao[1] **and L Bernal**[2]

[1] INFIP-CONICET, and Physics Department (FCEN-UBA), Ciudad Universitaria, Pab. I, 1428 Buenos Aires, Argentina
[2] Physics Department (FCEYN-UNMDP), Complejo Universitario, Funes y Peña, 7600 Mar del Plata, Argentina

E-mail: bilbao@df.uba.ar

Received 18 August 2009, in final form 29 January 2010
Published 21 May 2010
Online at stacks.iop.org/PSST/19/034024

Abstract
The scope for developing the present numerical method was to perform parametric studies for optimization of several configurations in magnetized plasmas. Nowadays there exist several efficient numerical codes in the subject. However, the construction of one's own computational codes brings the following important advantages: (a) to get a deeper knowledge of the physical processes involved and the numerical methods used to simulate them and (b) more flexibility to adapt the code to particular situations in a more efficient way than would be possible for a closed general code. The code includes ion viscosity, thermal conduction (electrons and ions), magnetic diffusion, thermonuclear or chemical reaction, Bremsstrahlung radiation, and equation of state (from the ideal gas to the degenerate electron gas). After each calculation cycle, mesh vertices are moved arbitrarily over the fluid. The adaptive method consists of shifting mesh vertices over the fluid in order to keep a reasonable mesh structure and increase the spatial resolution where the physical solution demands. The code was a valuable tool for parametric study of different physical problems, mainly optimization of plasma focus machine, detonation and propagation of thermonuclear reactions and Kelvin–Helmholtz instabilities in the boundary layer of the terrestrial magnetopause.

(Some figures in this article are in colour only in the electronic version)

1. Introduction

The general scope for developing the present numerical method was to perform parametric studies for optimization of several problems in plasma physics. Nowadays there exist several efficient numerical codes in the subject. However, the construction of one's own computational codes brings the following important advantages: (a) to get a deeper knowledge of the physical processes involved and the numerical methods used to simulate them and (b) more flexibility to adapt the code to particular situations in a more efficient way than would be possible for a closed general code.

Requirements for parametric studies are (a) the code should be run many thousand times, (b) does not need high precision, (c) has flexibility for adding or removing different physical phenomena and (d) parallel algorithms are desired.

We developed an Arbitrary Lagrangian–Eulerian (ALE) Finite Volume algorithm based on a previously reported code [1]. A three-dimensional (3D), time depend, multi-component, two-temperature code was used. The code includes ion viscosity, thermal conduction (electrons and ions), magnetic diffusion, thermonuclear or chemical reaction, Bremsstrahlung radiation, and equation of state (EOS) (from the ideal gas to the degenerate electron gas).

The main scope of this study was, on one hand, to give an approximate description of the scaling law of the thermonuclear reactions in a plasma focus (PF) discharge, and, on the other hand, to explore the optimal conditions for generation and propagation of thermonuclear reactions in a cylindrical fiber (Z-pinch).

2. Numerical method

We have used an ALE Finite Volume method with hexahedral cells that move at arbitrary velocity. The notation and definition of the geometry are described elsewhere [1]. The

main advantage of this method is that the geometry is imposed on the cells and not on the operators.

This method consists of integrating conserved quantities over a cell. For a general fluid property Ψ, the following identity holds:

$$\frac{\mathrm{d}}{\mathrm{d}t}\int_{V(t)}\Psi\,\mathrm{d}V=\frac{\partial}{\partial t}\int_{V(t)}\Psi\,\mathrm{d}V+\oint_{S(t)}\Psi\boldsymbol{w}\cdot\mathrm{d}\boldsymbol{S},\quad(1)$$

where integration is performed over a cell of arbitrary volume $V(t)$ with boundary $S(t)$ moving at an arbitrary speed $\boldsymbol{w}$. By choosing $\boldsymbol{w}=0$, that is both V and S remain fixed, a full Eulerian formulation is retrieved. On the other hand, setting $\boldsymbol{w}=\boldsymbol{v}(\boldsymbol{x},t)$—fluid velocity—leads to the standard Lagrangian formulation. The adaptive method consists of choosing an appropriated $\boldsymbol{w}(\boldsymbol{x},t)$ over the fluid in order to keep a reasonable mesh structure and increase the spatial resolution where the physical solution demands.

For the ideal MHD, the integral equations for mass (M), momentum ($\boldsymbol{P}$), internal energy (E) and magnetic flux (Φ) are

$$\frac{\mathrm{d}M}{\mathrm{d}t}=\frac{\mathrm{d}}{\mathrm{d}t}\int_{V(t)}\rho\,\mathrm{d}V=-\oint_{S(t)}\rho\,(\boldsymbol{v}-\boldsymbol{w})\cdot\mathrm{d}\boldsymbol{S},\quad(2)$$

$$\frac{\mathrm{d}\boldsymbol{P}}{\mathrm{d}t}=\frac{\mathrm{d}}{\mathrm{d}t}\int_{V(t)}\boldsymbol{v}\rho\,\mathrm{d}V=-\oint_{S(t)}\rho\boldsymbol{v}\,(\boldsymbol{v}-\boldsymbol{w})\cdot\mathrm{d}\boldsymbol{S}-\int_{S(t)}p\,\mathrm{d}\boldsymbol{S}+\int_{V(t)}\boldsymbol{j}\times\boldsymbol{B}\,\mathrm{d}V,\quad(3)$$

$$\frac{\mathrm{d}E}{\mathrm{d}t}=\frac{\mathrm{d}}{\mathrm{d}t}\int_{V(t)}\varepsilon\rho\,\mathrm{d}V=-\oint_{S(t)}\rho\varepsilon\,(\boldsymbol{v}-\boldsymbol{w})\cdot\mathrm{d}\boldsymbol{S}+\int_{S(t)}\left(\frac{c_pkT}{e}\boldsymbol{j}\right)\cdot\mathrm{d}\boldsymbol{S}-\int_{V(t)}p\nabla\cdot\boldsymbol{v}\,\mathrm{d}V,\quad(4)$$

$$\frac{\mathrm{d}\Phi}{\mathrm{d}t}=\frac{\mathrm{d}}{\mathrm{d}t}\int_{\Sigma(t)}\boldsymbol{B}\cdot\mathrm{d}\boldsymbol{S}=-\oint_{C(t)}\mathrm{d}\boldsymbol{l}\cdot\boldsymbol{E}'+\oint_{C(t)}[(\boldsymbol{v}-\boldsymbol{w})\times\boldsymbol{B}]\cdot\mathrm{d}\boldsymbol{l},\quad(5)$$

where ρ is the mass density, p the pressure, T the temperature, $\boldsymbol{j}$ the electrical current density, $\boldsymbol{E}'$ the electric field in the plasma frame of reference, $\boldsymbol{B}$ the magnetic field, $\varepsilon=p/\rho(\gamma-1)$ the internal energy density (c_p is the specific heat at constant pressure and γ the adiabatic constant) and e the charge of the electron. In the last equation Σ is an arbitrary open surface bounded by a closed path C, which moves according to $\boldsymbol{w}(\boldsymbol{x},\,t)$.

The integration domain is represented by a structured irregular mesh, with fixed connectivity made of hexahedral cells. Each cell is surrounded by six faces and eight vertices. Lagrangian cell methods are not adequate for describing flows undergoing severe deformations. Nuclear burning or combustion structures may present steep gradient of temperature, species concentration and heat release. The adaptive method consists of shifting mesh vertices over the fluid in order to keep a reasonable mesh structure and increase the spatial resolution where the physical solution demands.

Fluid variables are assigned to staggered locations in the mesh. Pressure, internal energy, density, species concentration, cell volume and mass are all assigned to cell centers. Coordinates $(x,\,y,\,z)$ and velocities $(u_x,\ u_y,\ u_z)$ are assigned to cell vertices. Appropriate mean values over adjacent cells or vertices are used when needed.

Global conservation of the above magnitudes is checked during calculation. Also, condition $\mathrm{div}(\boldsymbol{B})=0$ is controlled over the whole integration domain.

The same method is applied for more complex modeling of plasmas, which includes ion viscosity, thermal conduction (electrons and ions), magnetic diffusion, chemical or thermonuclear reactions, Bremsstrahlung radiation and realistic EOS from the ideal gas to the degenerate electron gas. The system of equations is based on a two-fluid model of plasma [2].

The time integration is sequential. This means that each process is integrated with a different uncoupled method during a time step. The overall truncation error is $O(\Delta\boldsymbol{x},\Delta t)$. Solution does not dependent on the integration order of the terms.

The calculation proceeds as follows:

- Hydrodynamics is integrated using a predictor–corrector method.
- Diffusion processes (of species concentration and energy) are integrated with alternating direction implicit (ADI) methods.
- Source terms from chemical or nuclear reactions are explicitly integrated in time.
- Mesh vertices are moved arbitrarily over the fluid. The rezone velocity with which vertices are moved over the fluid is calculated in order to increase spatial resolution where steep temperature gradients and high chemical/nuclear heat release are produced.

3. Scaling of a PF device

Self-constricted plasma configurations occur in a number of situations, including geophysics (lightning) and astrophysics (current channels at galactic scales). PF and Z-pinch are machines based on this principle. They are an interesting source of pulsed radiation (including thermonuclear reactions) with a broad utility in many technological applications.

PF 2D fluid codes were available more than 30 years ago [3, 4]. The finite volume method was first applied for simulating a hollow gas-puff Z-pinch [2]. Improvements in computer hardware allowed the extension to 3D. The scope of this study was to obtain an approximated description of the scaling law of the thermonuclear reactions in a PF discharge.

The PF dynamics is usually divided into four stages (or phases): breakdown, run-down, convergence and pinch (or focus). After breakdown a current sheath (CS) develops starting the run-down phase. The magnetic field pushes forward the CS against a neutral gas. After the traveling profile arrives at the end of the electrodes, the CS starts a convergence to the axis. During the convergence phase, both the magnetic piston and the shock wave move toward the axis. The pinch phase starts when the shock reflects off the axis. Since the magnetic piston continues converging, a further compression

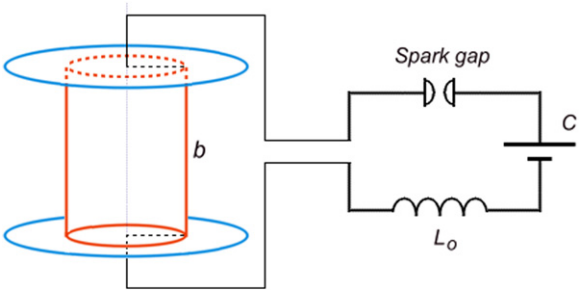

Figure 1. Plasma–electrical circuit coupling. A boundary path b is used.

and heating of the plasma occurs until the reflected shock hits the piston. This stage is usually called 'first compression'.

Due to the fact that the magnetic piston is not a straight cylinder, the maximum compression occurs at different times for different axial positions, leading to the development of $m = 0$ instabilities that produce several necking (called 'second compression' or necking phase).

Nuclear reaction and x-ray emission are produced in the pinch phase. The mechanism of nuclear reaction of a PF device still remains unclear. At least three different mechanisms can be devised: thermonuclear production along the whole column as a result of conversion of kinetic energy into internal energy during the first compression, thermonuclear production due to the development of instabilities and further heating (i.e. anomalous resistivity), and beam–target mechanism that can also have different contributions (for example, trapped ions in the pinch or ion beam against the neutral gas). There are many characteristics that are particular for each mechanism: anisotropy, maximum of the neutron production as a function of the filling pressure, scaling with the current, ratio between pure deuterium (DD) and deuterium–tritium (DT) outputs, influence of contaminants, etc. It is possible that the above-mentioned three mechanisms may share one or more of these properties, but quite probably they cannot share all of them. Numerical simulation can predict the expected values of these properties.

The set of plasma equations was coupled to the electrical circuit equation, through (see figure 1)

$$\frac{\mathrm{d}\left(\left(L_0 + L_b\right) I\right)}{\mathrm{d}t} = \frac{Q}{C} - RI + V_{\mathrm{sg}}(t) - \oint_b \mathrm{d}\boldsymbol{l} \cdot \boldsymbol{E}', \qquad (6)$$

where Q is the charge of the capacitor bank, C the capacity, L_0 and R the inductance and the resistance of the (concentrated) circuit, respectively, V_{sg} the voltage drop at the spark gap, L_b the inductance calculated at the pinch plasma boundary (b refers to the plasma boundary) and I the current. Finally, the magnetic field at the boundary and the current are related through

$$B_b\,(t, z) = \frac{\mu_{\mathrm{o}} I\,(t)}{2\pi r_b\,(t, z)}. \qquad (7)$$

In order to characterize the neutron production of the first compression thousands of numerical runs must be performed to cover an ample range of the initial parameters.

During convergence the CS is Rayleigh–Taylor unstable. In order to adequately describe the fastest growing instability

Table 1. List of parameters (a: inner radius, b: outer radius, l: anode length, C: bank capacity, L_0: external inductance, V: charging voltage).

Case	a (cm)	b (cm)	l (cm)	C (μF)	L_0 (nH)	V (kV)
BA	1.80	3.60	12.0	10.50	31	20–40
NE	3.30	6.25	21.0	225.00	20	15–25
SP	2.50	7.00	6.5	1.56	40	120–220
FR	8.00	12.00	56.0	1250.00	16	20–40
BR	1.65	4.50	13.5	30.50	100	21

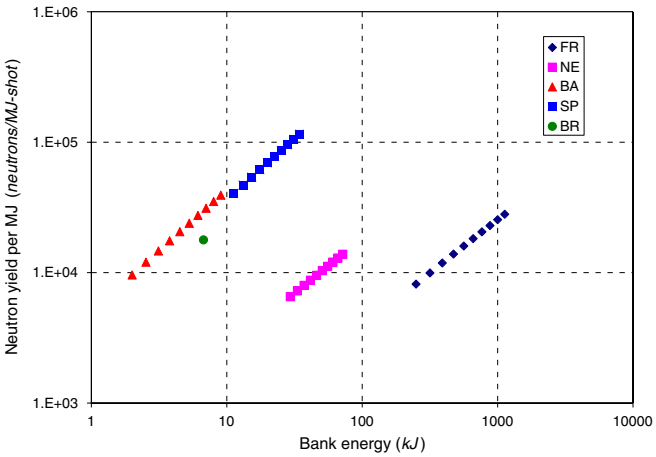

Figure 2. Neutron production per megajoule versus bank energy.

(that depends on the filling pressure, see, for example, [5]) the number of cells was between a minimum of 262 144 and a maximum of 1 048 576.

We have used data from five different PF, namely, PFII (BA), Nessi (NE), Speed (SP), Frascati (FR) and Brasimone (BR). The main parameters are (see table 1): anode length l and radius a, cathode radius b, bank capacity C, external inductance L_0, charging voltage V_0, initial filling pressure (p_0) and the gas type (only pure D_2 were used in the present calculations). These machines were selected because they cover an ample range of energy and velocity, and results from them are readily available in the literature. Among these machines, Brasimone PF is the only one that worked in a repetitive fashion.

Calculations proceed as follows. For each case and for each possible value of V_0 the initial filling pressure is browsed until the maximum neutron yield is obtained.

An interesting result is the neutron output per unit energy as a function of bank energy (figure 2). It is apparent from this plot that larger PF devices are less efficient. In order to clarify this point we plot in figure 3 the mean energy per particle and in figure 4 the ratio between ion and electron temperature at the end of the first compression phase. During convergence and compression the ions are heated by a shock wave, while electrons are heated by collisions with ions and atoms (joule heating is less important before the development of instabilities). From figure 4 it is apparent that at high energies the equipartition time is relatively smaller than that obtained at low energies, thus the ions are expected to be relatively cooler. This means that high energy machines are less efficient in neutron production than smaller machines.

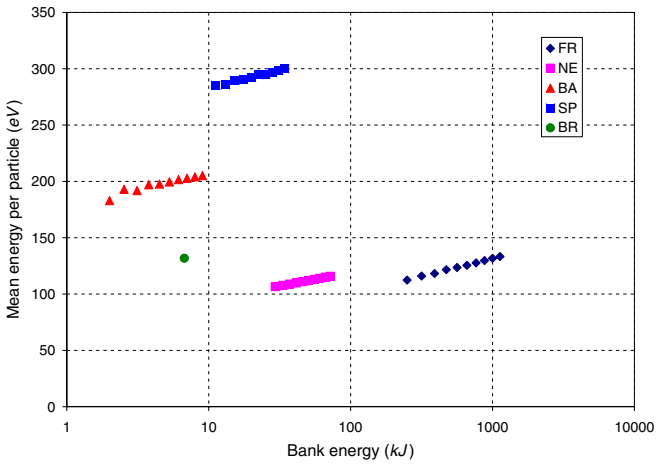

Figure 3. Mean energy per particle versus bank energy (E_c).

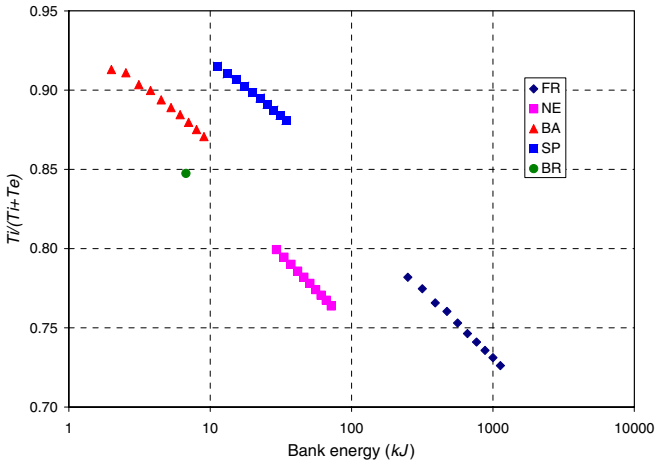

Figure 4. Temperature ratio ($T_i/T_i + T_e$) versus bank energy (E_c).

This fact seems to be linked to the necessary relation, set by construction, between the parameters that prevents optimizing all stages at the same time.

The numerical simulation was a useful tool for the parametric study of a PF. For example, it helped to understand the important role of the equipartition time on the neutron production.

The cooling effect of the equipartition time should not be confused with the drastic drop in neutron production that happens at higher energies. A possible explanation, based on the results from the 2D code, is that assuming that 'good' and 'bad' breakdown regions are separated by the line $p_o \propto V_o$ [6] then always will be 'crossed' by the pressure of maximum production, $p_o \propto V_o^2$, at higher energies. This behavior is confirmed by the present parametric study, which means that the standard PF configuration cannot be simultaneously optimized for breakdown and nuclear production.

4. Generation and propagation of thermonuclear reactions

The idea of a simple nuclear reactor based on a Z-pinch has been discarded because the heating of a whole plasma column to high temperatures will require unrealistic energy input for the plasma heating [7–10]. Another approach [11] to the production of a positive energy yield consists of a small pinch zone heated to high temperature only. Experiments on Z-pinches always concern low and high temperatures and high-density plasma regions that arise spontaneously in Z-pinch necks. A burn wave might be initiated in the Z-pinch column if in one of these small plasma regions a Lawson-like condition is fulfilled. The nuclear energy, which is produced because of a burn wave spread, is controllable and is sufficient for the compensation of energy losses for the pinch production. 2D simulations of a D–T nuclear detonation inside a cylindrical liner have been performed by Avrorin *et al* [12].

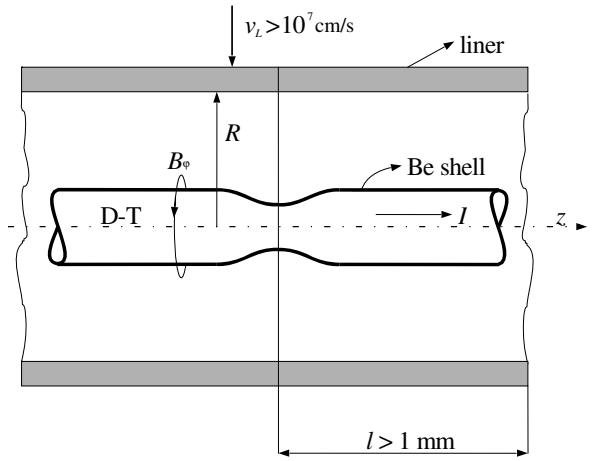

Figure 5. Implosion of cylindrical liner on a Z-pinch.

Perhaps the most promising application of liner implosions is the volume or spark ignition in cylindrical plasma. A cylindrical liner can successfully confine a magnetized, hot plasma column [13–15]. The technical parameters necessary for inertial confinement fusion (ICF) applications (in particular, volume and spark ignition in plasma compressed by an imploding liner) have been investigated through numerical simulations. These calculations provide an insight into the structure of the liner and the plasma and indicate the range of parameters required for ignition and detonation in such a liner-pinch system.

In order to investigate the ignition criteria it is necessary to perform numerical simulations using a realistic plasma fluid model and corresponding transport coefficients. Transport and viscosity coefficients are taken from [16] and the fusion cross sections from [17].

The studied approach is based on a spark created in a neck of a dense Z-pinch. The neck is formed as a result of an $m = 0$ instability starting from an initial small $m = 0$ axial perturbation. The advantage of this approach is that the spark can be programmed to occur at the moment of maximum pinch current at the correct place and time by choosing suitable initial configuration. The disadvantage is that one must provide an initial magnetic flux and the associated current I_0 and that the current rise time must be short. A possible way of getting adequately short rise time is the compression of a magnetic flux of a Z-pinch by a fast imploding liner (figure 5).

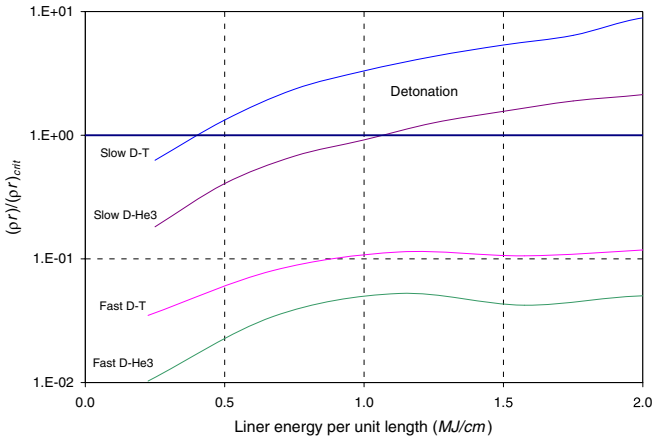

Figure 6. Detonation criteria for slow and fast liner for D–T and D–He_3 plasma. Fast liners do not provide enough inertia to confine the plasma up to the detonation conditions.

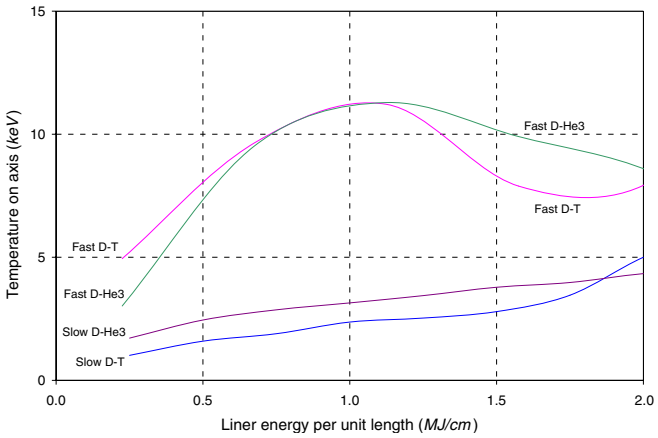

Figure 7. Temperature on pinch axis for slow and fast liners in D–D and D–He_3 plasma.

The spark created in the neck of a dense Z-pinch can ignite a fusion detonation in the adjacent D–T plasma channel. An $m = 0$ instability of a Z-pinch carrying a current of the order of 10 MA, with a rise time inferior to 10 ns can generate a spark capable of igniting a fusion detonation in the adjacent D–T plasma channel. Such a μZ-pinch may be produced by a fast implosion of a cylindrical liner, while a conical channel properly chosen can amplify the spark energy. In order to derive some general rules for the parameters of the spark, the transition, the cylinder of advanced fuel and the liner different numerical models were used.

One interesting study is relative to the liner mass and velocity. We have used several initial velocities for the liner ranging from slow liners ($v = 2 \times 10^6\,\mathrm{cm\,s^{-1}}$) to fast liners ($v = 3 \times 10^7\,\mathrm{cm\,s^{-1}}$).

Note that at the same kinetic energy value of the liner, the slow one provides a larger tamping effect than the faster one, while the faster one produces a larger temperature rise in the pinch than the slow one.

In the following example, the initial pinch parameters are radius $a = 0.2$ cm, temperature $T = 30$ eV, linear density $N = 5.2 \times 10^{19}\,\mathrm{part\,cm^{-1}}$. The initial current was $I = 1$ MA. In order to adequately describe the smallest, fast growing $m = 0$ instability a cylindrical $(r,\ \varphi,\ z)$ mesh of $91 \times 32 \times 181$ cells was used.

In D–T the condition for detonation propagation is fulfilled at $0.5\,\mathrm{MJ\,cm^{-1}}$ liner kinetic energy level (see figure 6). D–He_3 plasma requires liner energies above $1.1\,\mathrm{MJ\,cm^{-1}}$ in order to reach detonation conditions. Note that the fast liner produces a larger temperature in the plasma (see figure 7). This has the effect of a premature thermonuclear output that inhibits a further compression. This means that both detonation and ignition are hard to reach using fast liners.

For detonation propagation the plasma does not have to be heated to the ignition temperature, and therefore the resulting energy required for detonation is much smaller than that for volume ignition. Provided the spark energy can be neglected with respect to the total energy, the spark ignition scheme is energetically much more advantageous than the volume ignition.

Slow liners can be useful for compressing the plasma up to the detonation propagation condition in both D–T and D–He_3. The liner energy required is about $1\,\mathrm{MJ\,cm^{-1}}$. At the same time, the development of the $m = 0$ instability creates a region where the ignition condition may be reached. At that point a thermonuclear detonation is triggered; it can then propagate along the pinch if adequate conditions have already been achieved. The numerical code can help in finding the best regime for this purpose.

5. Conclusions

The numerical simulation was a powerful tool for the parametric analysis of pinch compression and development of a nuclear burning in a cylindrical fiber.

The sequential implementation feasibility deserves to be mentioned. This turned out to be of practical use, because each physical process is treated with a different numerical method. In this way it is easy to modify the code since adding or suppressing physical processes can be simply done by adding or canceling isolated numerical procedures.

The improved hydrodynamics method worked well in a broad range of Mach number from subsonic (10^{-3}) to supersonic.

The time step was not restricted by stability conditions. It was restricted by efficiency considerations: using a larger time step, the explicit calculation progresses faster, but the implicit stage of the hydrodynamic requires more iterations. An optimum time step has been used for which computational effort is minimum.

Acknowledgments

This work is partially supported by CONICET (Argentina).

References

[1] Bilbao L 1990 *J. Comput. Phys.* **91** 361
[2] Bernal L and Bilbao L 1998 *Nuovo Cimento* **20** 661–74
[3] Potter D E 1971 *Phys. Fluids* **14** 1911–24
[4] Maxon S and Eddleman J 1978 *Phys. Fluids* **21** 1856–65

[5] Bilbao L and Bruzzone H 1984 *Phys. Lett.* A **101** 261
[6] Gourlan C, Kroegler H, Maisonnier Ch, Rager J P, Robouch B, Bertalot L, Gentilini A, Arcipiani B, Pedretti E and Steinmetz K 1978 *Proc 2nd Int. Conf on Energy Storage Compression and Switching (Venice, 5–8 December 1978)* ed V Nardi, H Sahlin and W H Bostick (New York: Plenum) p 221
[7] Artsimovich L A 1964 *Controlled Thermonuclear Reactions* (New York: Gordon and Breach)
[8] Bakshaev Yu L *et al* 2000 *Czech. J. Phys.* **50** (Suppl.) 121–6
[9] Batunin A V, Bulatoy A N and Vikharev V D 1990 *Fiz. Plasmy* (*Sov. Plasma Phys.*) **16** 1027–35
[10] Gol'berg S M, Liberrnann M A and Velikovich A L 1990 *Plasma Phys. Control. Fusion* **32** 319–26
[11] Ryutoy D D, Derzon M S and Matzen M K 2000 *Rev. Mod. Phys.* **72** 167–223
[12] Avrorin E N *et al* 1984 *Fiz. Plasmy* **10** 514
Avrorin E N *et al* 1984 *Sov. J. Plasma Phys.* **10** 298
[13] Maisonnier Ch *et al* 1965 *Proc. 2nd IAEA Conf. on Plasma Physics and Controlled Nuclear Fusion Research (Culham, UK)* vol 2 (Vienna: IAEA) p 345
[14] Bortolotti A *et al* 1994 *Proc. 3rd Int Conf. on Dense Z-Pinches (London, 1993)* (AIP Conf. Proc.) (New York: AIP) vol 299, p 372
[15] Degnan J H *et al* 2001 *IEEE Trans. Plasma Sci.* **29** 93
[16] Bilbao L and Linhart J G 1996 *Plasma Phys. Rep.* **22** 457
[17] Bosch H S and Hale G M 1992 *Nucl. Fusion* **32** 611